



Research article

The climate adaptive characteristics of urban inside/outside water bodies based on their cooling effect in Poyang and Dongting lake regions, China

Zhigang Deng^{a,b}, Hongmei Zhao^{b,*}, Lin Li^b, Guihua Liu^b, Hui Lin^b, Adam Thomas Devlin^b

^a School of Software, East China Jiaotong University, Nanchang, PR China

^b Key Laboratory of Wetland and Watershed Research, Ministry of Education/School of Geography and Environment, Jiangxi Normal University, Nanchang, PR China



ARTICLE INFO

Keywords:

Climate adaption
Distance weighted area index (DWAI)
)
Cooling effect of water bodies (WCE)
Inland large lakes
Urban heat island (UHI)

ABSTRACT

Most publications have focused on the cooling effect of urban inside water bodies. However, the climate adaptive characteristics of urban inside/outside water bodies is seldom studied. In this paper, three types of water bodies, i.e., urban inside water bodies, urban outside discrete water bodies and large water bodies are identified according to their relative spatial relationships with built-up areas. The climate adaptive landscape characteristics of water bodies are analyzed based on water bodies' cooling effect (WCE) inside and outside cities in the Poyang Lake and Dongting Lake regions. Seventy-three Landsat TM/OLI/TIRS images acquired from 1989 to 2019 are employed. Landscape scale characteristics of urban inside/outside water bodies are described by area, water depth, perimeter to area ratio (PARA) and distance-weighted area index (DWAI). Three temperature-related parameters are calculated to estimate the WCE in different conditions. Climate adaptive characteristics of water bodies inside/outside cities are determined by correlation and regression analysis. Results show that: 1) The long river shape, depth, orientation and fluidity of urban inside water bodies are benefit to enhance their cooling effect; 2) the distance of urban outside water bodies from built-up areas are positive correlated with their cooling effect; 3) the optimal acreage of large water bodies are >2500 km² and 1111–1287.5 km² for climate adaption of Poyang Lake and Dongting Lake, respectively. Simultaneously, the WCE of urban outside large water bodies is related with human activities and climate conditions. The results of our study provide a significant contribution to blue-space planning in cities, and provide insights into actionable climate adaption planning in inland large lake areas.

1. Introduction

Urban heat island (UHI) effect has been a concern for decades due to rapid urbanization [1,2]. Simultaneously, how to mitigate UHI effect is another issue of considerable interest. Urban green and blue spaces (i.e. water bodies) play major roles in effectively alleviating the UHI effect [3–6]. The amount of green and blue space has a significant influence on UHI, environmental quality, quality of

* Corresponding author. Key Laboratory of Wetland and Watershed Research, Ministry of Education/School of Geography and environment, Jiangxi Normal University, Nanchang, 330022, PR China.

E-mail address: zhm8012@tom.com (H. Zhao).

<https://doi.org/10.1016/j.heliyon.2023.e15974>

Received 18 April 2023; Received in revised form 27 April 2023; Accepted 28 April 2023

Available online 1 May 2023

2405-8440/© 2023 Published by Elsevier Ltd. This is an open access article under the CC BY-NC-ND license (<http://creativecommons.org/licenses/by-nc-nd/4.0/>).

life and human health in urban areas [7–10]. The study of UHI effect has been investigated in an exponentially increasing manner from 1997 to November 2022. Over 41% of UHI-related articles have discussed the cooling effect of water bodies (Fig. 1). It is observed that only 0–5 literatures on cooling effect of green and/or water bodies were found before 1997, and little changes observed from 1990 to 1997. Therefore, literatures on cooling effect of UHI and water bodies before 1997 are not discussed in this work.

It is reported that spatial patterns of green-blue spaces have a significant influence on their cooling effect. Urban wetland, as the special green-blue spaces, whose cooling effect is regarded as an important ecosystem regulating service [11–15]. Wetland shape and location are significant indicators influencing urban temperature [16]. The cooling effect of urban wetland varies in different urban rural belts [17]. The closer that wetlands are located to urban center, the more significant the regulation on temperature will be [12]. The littoral forest yielded more significant cooling effect than that of the separate trees [18]. However, the impact of water body area ratio on park cooling effect was not significant for a little park [19].

Water bodies have long been used as essential design tools for scientific planning to control the urban temperature [20–22]. The cooling effect of water bodies is much more efficient than tree-based green spaces in subtropical cities [23,24]. The cooling effect of water bodies is mainly influenced by their size and spatial patterns [25]. For example, a negative logarithmic relationship exhibits between urban water body size and its mean land surface temperature [26–28]. The water bodies size and their distance from built-up areas are positively and negatively correlated with the urban cooling effect, respectively [29]. The cooling effect of water bodies is the most pronounced within 1 km (horizontal distance) [13], and it changes with distance [30]. Urban water bodies located near city center can deteriorate the nighttime cooling effects due to elevated humidity [31]. Additionally, the surrounding land cover has a greater influence than water bodies on the overall cooling effect [32].

The cooling effect of water bodies varies with climatic conditions, including, time of day, season, temperature, wind speed, solar radiation etc. [33–38]. Wind speed plays a major role both in terms of cooling capacity and area of influence [39]. Higher solar radiation and lower wind conditions may further enhance the cooling effect [35].

Previous investigations have focused on the cooling effects of small water bodies on microclimate at patch size and micro-landscape scales [40–42]. However, there has been a lack of investigations on the climate adaptive characteristics of urban outside water bodies at the regional scale. Water bodies' contribution to the urban climate is still a distinct knowledge gap [36]. The quantitative role of water bodies is still uncertain for climate adaptive [43]. In this paper, climate adaptive characteristics of water bodies are analyzed based on WCE in the Poyang Lake and Dongting Lake regions. Three types of water bodies are classified according to their relative distance from the built-up area, including urban inside water bodies (e.g., lakes and rivers), outside discrete small water bodies, and large water bodies (e.g., Poyang Lake and Dongting Lake). Urban inside water bodies refer to the water bodies within 1 km distance from the boundary of built-up area. Outside discrete small water bodies, which are located between the urban inside water bodies and the large lakes, are found in both the Poyang Lake and Dongting Lake regions.

2. Study area and data

2.1. Study area

Poyang Lake (28°22'–29°45'N and 115°47'–116°45'E) and Dongting Lake (28°30'–30°20'N and 113°10'–114°40'E) are the largest and second largest inland fresh water lakes in China, found in the middle and lower reaches of Yangtze river (Fig. 2(a)). Dongting Lake is divided into three sub-lakes, including east, south and west. East and south Dongting lake are included in this study. The agricultural activities occurred in the Poyang Lake region are similar with those in Dongting Lake region.

Nanchang and Changsha are the largest cities in Poyang Lake and Dongting Lake regions, respectively, which located in subtropical monsoon climate zones (Fig. 2(b) and (c)). There is little difference between Nanchang and Changsha for the monthly mean climatic characteristics, including sunny days, mean temperature and mean wind speed (Fig. 3). However, the wind direction of daily

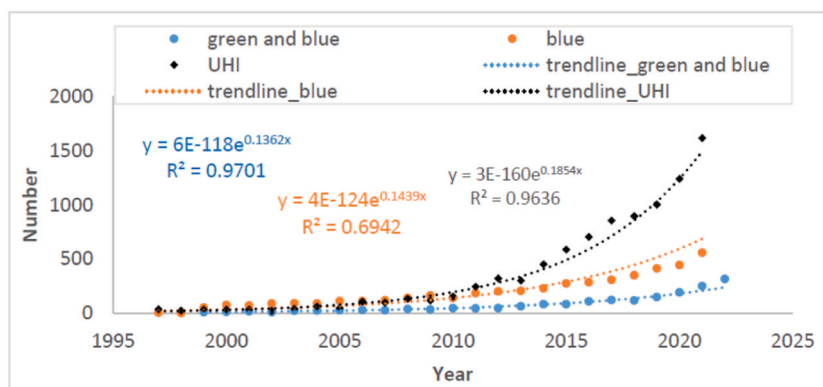


Fig. 1. Number of articles focused on the “cooling effect of green and blue space in urban areas” and UHI from 1997 to Nov. 2022 (Literature parameters are from the ScienceDirect database). (For interpretation of the references to colour in this figure legend, the reader is referred to the Web version of this article.)

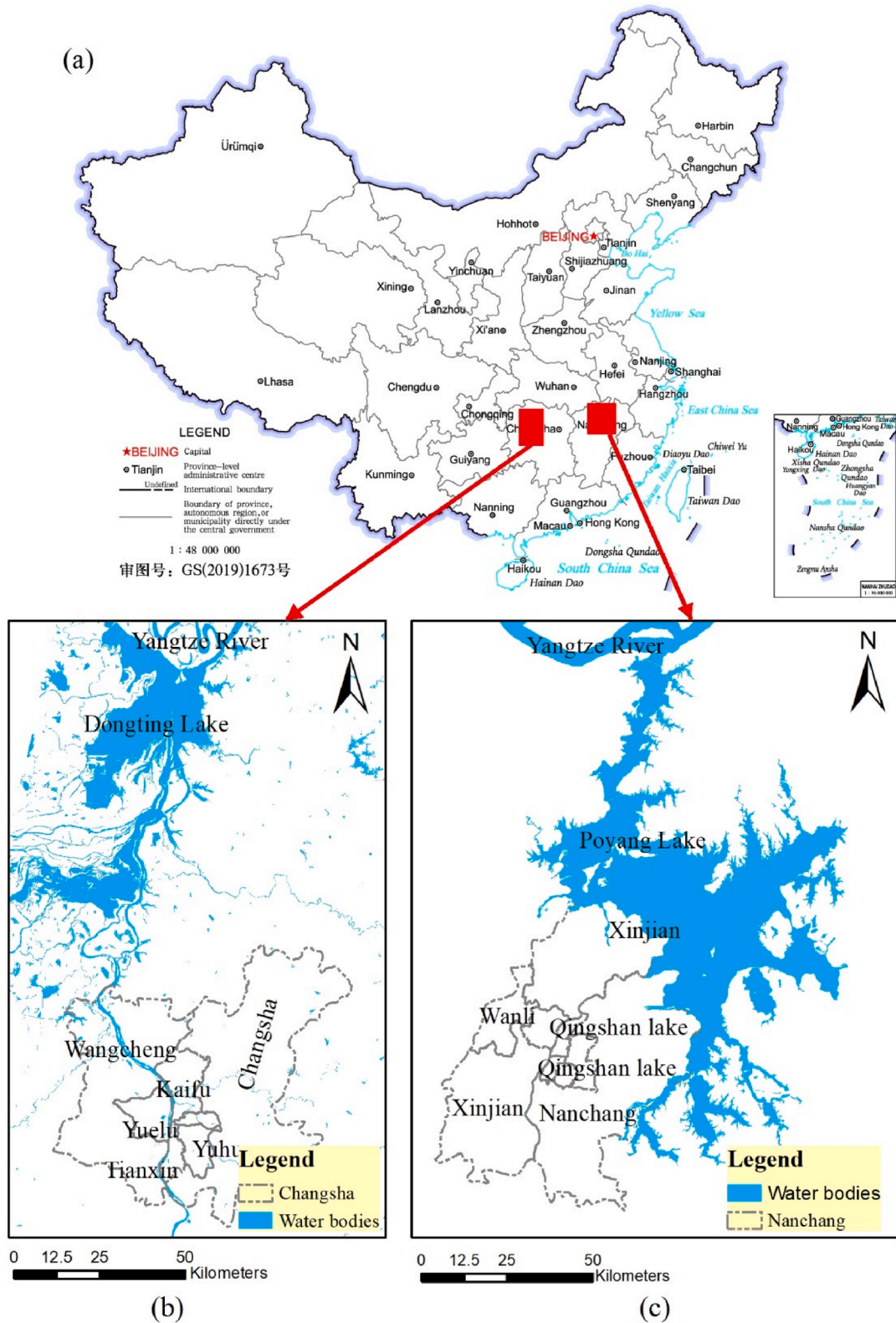


Fig. 2. Study area: (a) Location of the study areas; (b) Dongting Lake region; (c) Poyang Lake region.

maximum wind speed is different between Nanchang and Changsha. Wind direction of Nanchang and Changsha are dominated by northeast and northwest, which might be affected by the orientation of Poyang lake and Dongting lake, respectively (Fig. 4(a) and (b)).

Both Nanchang and Changsha have been experienced rapid urbanization from 1990 to 2020. However, the urbanization speed of Changsha is significantly higher than that of Nanchang. Nanchang have been designed as waterfront city surrounded by rivers and lakes from 2001 to 2020. Changsha have been built as mountainous and water city characterized by one river and two banks due to 2010. And then the Urban Planning Version 2003–2020 of Changsha is revised in 2014 to double urban planning area, named “multiplication plan of Changsha urban planning”.

The landscape patterns of water bodies inside/outside Nanchang are different from that inside and outside Changsha, when the water bodies are mapped into three types. Several urban inside lakes exist in Nanchang, which changes with the expansion of the built-up area. However, there are much less urban inside lakes in Changsha, which is discussed more in Section 4.1.1 below. Simultaneously, Gan River and Xiang River flow through Nanchang and Changsha, respectively. And then, the density of discrete water bodies outside Nanchang is much higher than that outside Changsha (Section 3.3). In a word, Poyang Lake and Dongting Lake regions provide natural test sites for us to analyze the climate adaptive landscape characteristics of water bodies.

2.2. Data

2.2.1. Remote sensing images

Landsat 5 TM and Landsat 8 OLI/TIRS images acquired on cloud-free days from 1989 to 2019 are used in this study. 31 and 42 Landsat images are used for the Poyang Lake (P121R040) and Dongting Lake (P123R040, P123R041) regions, respectively. The cloud cover percentage for the chosen scenes are less than 5%. The temporal distribution of the selected Landsat TM/OLI/TIRS images are provided in Table 1. Additionally, SRTM DEM digital elevation product (SRTM V3 from “USGS/SRTMGL1_003”) and Sentinel 1 SAR GRD image collection (“COPERNICUS/S1_GRD”) acquired in 2020 are used in this study. SRTM and Sentinel 1 SAR data have spatial resolutions of 30 m and 10 m, respectively.

2.2.2. Land use cover maps and statistical data

Land use cover type maps from 1989 to 2019 in Poyang Lake and Dongting Lake are used in the study. Seven land use/cover types were mapped, namely, water bodies, built-up area, development (inc. bare sandy land and river beach), cropland, forest, lake beach, grassland. The spatial resolution of Land use/cover type maps are 30 m. The overall accuracy of classifications was larger than 85% (Tables 2 and 3). All the selected datasets are rectified to WGS84, Universal Transverse Mercator (UTM) coordinate system. Additionally, statistical meteorological data from 2001 to 2019 are used to delineate the climate characteristics of the study area.

3. Methods

The variables, which are used to represent landscape scale characteristics, are acreage ratio of water to built-up (AR_{wb}), water depth, perimeter to area ratio (PARA), acreage and the distance-weighted area index (DWAI). The AR_{wb} , water depth and PARA are used to delineate urban inside water bodies. DWAI and acreage of the large lakes are used for quantifying the landscape scale characteristics of water bodies outside cities. WCE is quantified by brightness temperature.

3.1. Landscape scale characteristics of water bodies

3.1.1. Acreage and perimeter to area ratio (PARA)

The acreage of water bodies varies with date and season in both the Poyang Lake and Dongting Lake regions. The MNDWI is calculated from multi-temporal Landsat images using the Google Earth Engine (GEE). The acquisition date of multi-temporal Landsat images is consistent with that of radiance temperature. The threshold value of MNDWI is then determined from 0.15 to 0.2 by

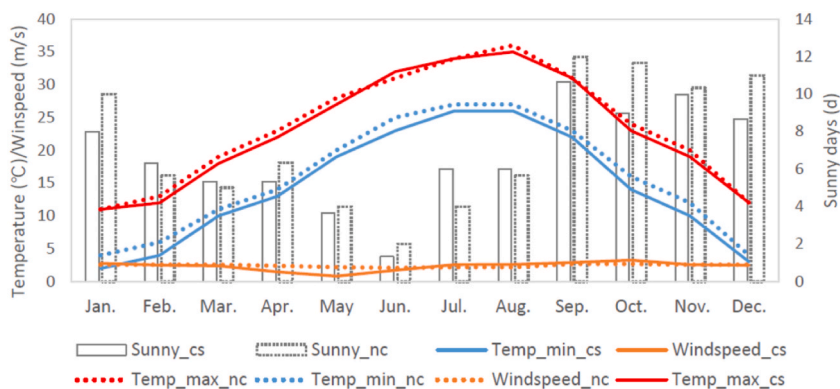


Fig. 3. Monthly mean meteorological characteristics of Changsha (cs) and Nanchang (nc) (2001–2019).

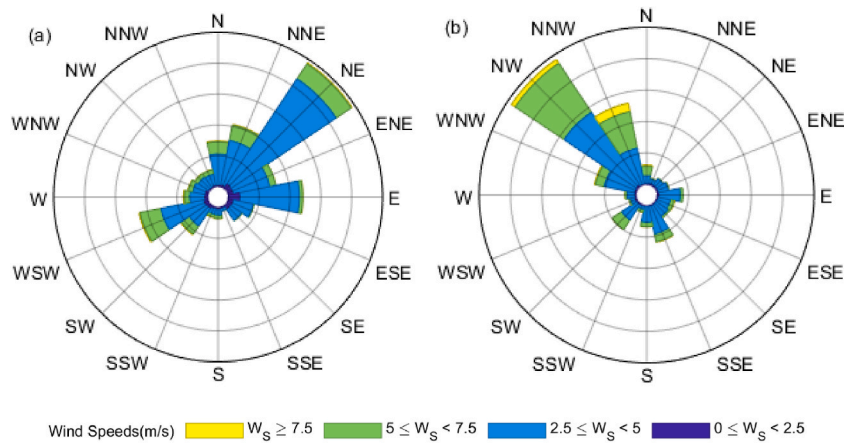


Fig. 4. Daily maximum wind rose (2001–2019): (a) Nanchang; (b) Changsha.

Table 1
Temporal distribution of the selected Landsat TM/OLI/TIRS images.

Sensor	Poyang Lake			Dongting Lake		
	AD of LUCC	NRT	Period	AD of LUCC	NRT	Period
Landsat 5 TM	Jul. 15th, 1989	1	1988–1989	Sep. 2nd, 1990	2	1989–1991
	Dec. 7th, 1995	3	1994–1996	Sep. 29th, 1994	2	1994–1995
	Nov. 2nd, 2000	6	1999–2001	Sep. 13rd, 2000	2	1999–2001
	Oct. 31st, 2005	8	2004–2005	Apr. 20th, 2005	7	2004–2006
	Mar. 19th, 2010	5	2008–2010	Nov. 12nd, 2010	2	2009–2011
Landsat 8 OLI/TIRS	Oct. 11th, 2015	3	2015–2016	Jul. 23rd, 2016	3	2015–2017
	Sep. 20th, 2019	5	2017–2019	Oct. 4th, 2019	3	2019

*AD of LUCC is the acquisition Date of Landsat images for land use/cover classification and the time of data acquisition is ~AM 09:00; NRT is the number of radiance temperature scenes; Period is the collection period of radiance temperature.

Table 2
Accuracy assessment of classification in Poyang Lake regions.

Types	1989	1995	2000	2005	2010	2015	2019
Water	91.04%	93.06%	91.67%	96.67%	87.27%	96.36%	95%
Built-up	88.41%	89.71%	87.14%	89.33%	94.29%	90.28%	85%
Development	89.55%	90.91%	92.73%	92.73%	90.91%	90.91%	86.36%
Forest	85.19%	85.71%	87.14%	92.31%	96.92%	85.94%	86%
Cropland	90.67%	88.73%	89.71%	90.00%	96.97%	92.73%	86%
Beach	90.91%	92.73%	85.71%	85.45%	85.45%	91.07%	91.38%
Grassland	–	90.91%	90.91%	94.55%	94.55%	93.10%	76.67%
Overall accuracy	89.13%	90.13%	89.17%	91.53%	92.64%	91.33%	86%
Kappa	0.8692	0.8846	0.8734	0.901	0.9139	0.8987	0.8381

Table 3
Accuracy assessment of classification in Dongting Lake regions.

Types	1990	1995	2000	2004	2010	2016	2019
Water	96.05%	98.63%	100.00%	94.03%	92.86%	90.14%	95%
Built-up	91.03%	88.61%	87.34%	85.71%	89.74%	87.67%	85%
Development	84.62%	91.07%	94.64%	87.27%	91.07%	85.25%	81.81%
Forest	91.55%	87.32%	91.18%	91.89%	94.37%	93.15%	86%
Cropland	89.71%	85.92%	88.16%	88.61%	86.67%	88.31%	83.75%
Beach	87.93%	88.14%	89.09%	85.45%	88.52%	83.64%	91.38%
Overall accuracy	90.38%	89.98%	91.54%	88.94%	90.51%	88.29%	85.67%
Kappa	0.8844	0.8793	0.8981	0.8668	0.8859	0.8592	0.8340

comparison between multi-spectral images and MNDWI to map water bodies in both Poyang Lake and Dongting Lake. And then, the acreage of water bodies is retrieved from each scene of water bodies. Acreage ratio between water bodies and built-up (AR_{wb}) is calculated by Eq. (1) to quantify the distribution of urban inside water bodies:

$$AR_{wb} = \frac{A_w}{A_b} \tag{1}$$

where A_w is the total acreage of water bodies within 1 km distance from built-up areas and A_b is the total acreage of built-up areas.

The PARA of urban inside water bodies are calculated from each scene of urban inside water bodies using ArcGIS software. PARA is a parameter used to describe the shape of water bodies. When the shape is circular, the PARA value is the smallest. The longer the shape is, the greater PARA is [44].

3.1.2. Water depth

The range of water depth is estimated by the lake/river bottom elevation difference between shallow and deep water bodies (Eq. (2)).

$$\text{Depth} = E_s - E_d \tag{2}$$

where Depth is the water depth, E_s is the lake/river bottom elevation of shallow water bodies, and E_d is the lake/river bottom elevation of deep water bodies. The shallow and deep water bodies are identified by the surface water cover frequency (SWCF) of urban wetland, which is calculated by Eq. (3). The shallow water has lower SWCF and deep water bodies refer the areas with higher SWCF.

$$SWCF = \sum_{i=1}^n w_i \tag{3}$$

where w_i is the thematic map of water bodies at the i th acquired date, n is annual SWCF of 2020 from Sentinel-1 SAR data.

The surface water extent of the study area could be extracted by Sentinel-1 Dual-Polarized Water Index (SDWI) (Eq. (4)), [45].

$$w_i = \ln(10 * VV_i * VH_i) - 8 \tag{4}$$

where, VV_i and VH_i represent Sentinel-1 C-band single polarized (VV) and double polarized (VH) images at the i th acquired date in 2020, respectively. w_i is Sentinel-1 Dual-Polarized Water Index. A constant threshold value (zero) is used to retrieve the surface water extent from SDWI. The surface water extent is retrieved by $SDWI > 0$.

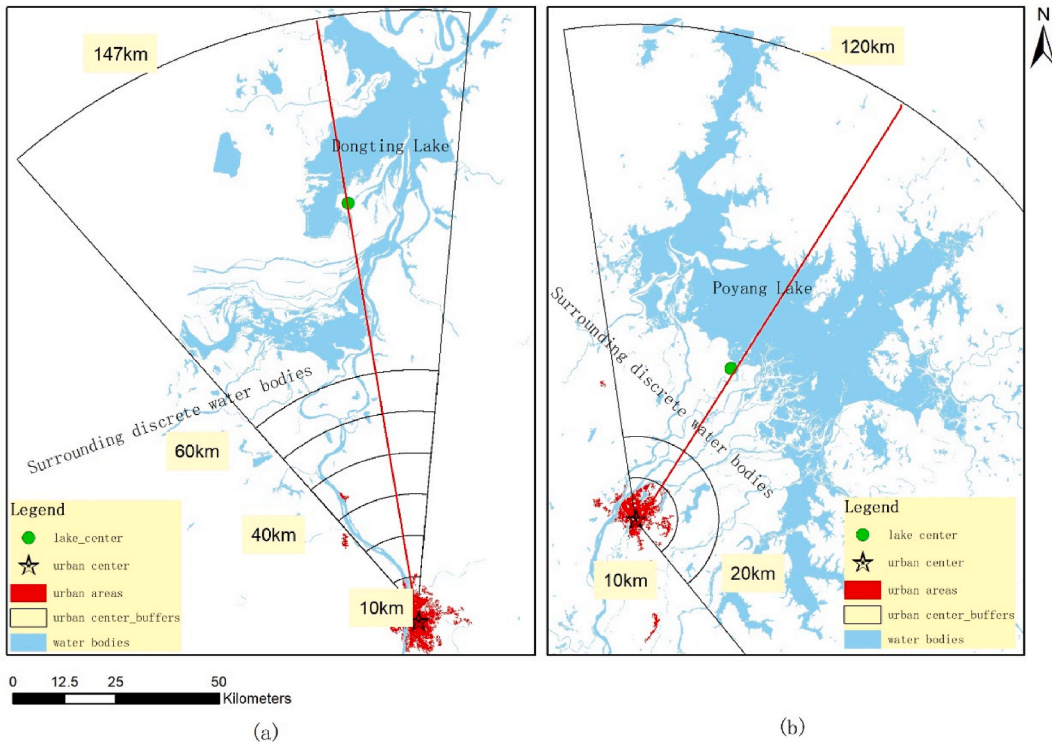


Fig. 5. Radial buffer zones for Dongting and Poyang Lakes. (a) Dongting Lake; (b) Poyang Lake.

3.1.3. The distance-weighted area index (DWAI)

Eight and four sub-zones are established in the Dongting Lake and Poyang Lake regions, respectively (Fig. 5(a) and Fig. 5(b)). Six and two 10 km buffer zones are set up between the geometric centers of built-up areas and large water bodies in the Dongting Lake and Poyang Lake regions, respectively (Fig. 5(a) and (b)). A larger buffer zone is determined between the minimum and maximum distance from the large lakes (Dongting and Poyang) to the geometric centers of the built-up areas. Then, discrete small water bodies around the large lakes and the large lakes themselves within the larger buffer zone are analyzed separately (Fig. 5). The angles of the sector in Fig. 5 are determined by the boundaries of Dongting Lake and Poyang Lake and the geometric centers of built-up areas in Changsha and Nanchang, respectively.

The mean distance-weighted area index (DWAI) is defined as an integrated index to quantify the spatial characteristics of discrete water bodies outside cities, expressed by Eqs. (5) and (6):

$$DWAI = \sum_{j=0}^m DWAI_j \quad (5)$$

$$DWAI_j = \frac{\sum_{i=0}^n A_{ij}}{d_j} \quad (6)$$

where DWAI is the distance-weighted area index of discrete water bodies, m is the number of spatial buffer bands, $DWAI_j$ is the distance-weighted factor of discrete water bodies in the j th buffer band, using $m = 1$ for the large lake buffer; A_{ij} is the area of outside discrete water bodies, n is the number of water bodies in the j th buffer band, d_j is the distance from the geometric center of water bodies in the j th buffer band to the geometric center of built-up areas. The geometric center of water bodies and built-up areas are determined using ArcGIS software in this work.

3.2. Quantification of WCE

3.2.1. Retrieval of brightness temperature

Satellite thermal infrared (TIR) images are used to evaluate the brightness temperature. The brightness temperature is retrieved from Landsat TIR images in two steps:

First, the digital numbers (DNs) of the thermal infrared bands are converted to radiation luminance for Landsat 5 and Landsat 8 (Landsat 5&8 Science Users' Handbook) TIR bands, respectively (Eqs. (7) and (8)).

For the Landsat 5 TIR band (i.e., band 6),

$$R_{TM6} = \frac{V}{255} (R_{max} - R_{min}) + R_{min} \quad (7)$$

where V represents the DN of band 6, R_{TM6} is the radiance of Landsat 5 TM band 6, R_{max} is the maximum radiance of Landsat 5 TM band 6 ($R_{max} = 1.896$ (mW* cm⁻² * sr⁻¹)), R_{min} is the minimum radiance of Landsat 5 TM band 6 ($R_{min} = 0.1534$ (mW* cm⁻² * sr⁻¹)).

For the Landsat 8 TIR bands (band 10)

$$L_\lambda = M_L Q_{cal} + A_L \quad (8)$$

where L_λ is top of atmosphere (TOA) spectral radiance (Watts/(m² * srad * μm)), M_L is the band-specific multiplicative rescaling factor from the metadata (RADIANCE_MULT_BAND_x, where x is the band number), A_L is the band-specific additive rescaling factor from the metadata (RADIANCE_ADD_BAND_x, where x is the band number), and Q_{cal} is the quantized and calibrated standard product pixel values (DN). Landsat 8 TIR band 10 is used in this section.

Then radiation luminance is converted to at-satellite brightness temperature in degrees Kelvin (K) by Eqs. (9)–(10)

For Landsat 5,

$$T = \frac{K1}{\ln(K2/(R_{TM6}/b) + 1)} \quad (9)$$

where $K1 = 1260.56$ K and $K2 = 60.766$ (mW* cm⁻² * sr⁻¹ μm⁻¹), which are pre-launch calibration constants, and b represents the effective spectral range; $b = 1.239$ (μm), when the sensor's response is much more than 50%.

For Landsat 8,

$$T = \frac{K2}{\ln(K1/L_\lambda + 1)} \quad (10)$$

where T is the at-satellite brightness temperature (K), L_λ is TOA spectral radiance (Watts/(m²*srad* μm)), $K1$ and $K2$ are the thermal conversion constants from the metadata ($K1_CONSTANT_BAND_x$ and $K2_CONSTANT_BAND_x$, where x is band number 10 or 11). Band 10 is used in Eq. (10).

3.2.2. Estimation of WCE in different conditions

Generally, the temperature of water bodies is seldom influenced by human activities. The temperature difference between built-up areas and water bodies (TD_{bw}) is used to evaluate the absolute WCE (Eq. (11)), which might be influenced by temporal/seasonal temperature.

$$TD_{bw} = T_{bu} - T_w \tag{11}$$

where TD_{bw} is the mean temperature difference between built-up areas and water bodies, T_{bu} is the mean temperature of built-up patches, and T_w is the mean temperature of water patches.

Season-independent WCE (RTD_{bw}) is calculated by Eq. (12) to eliminate the temporal/seasonal effect and the influence of human activities.

$$RTD_{bw} = (T_{bu} - T_w) / T_m \tag{12}$$

where RTD_{bw} is the season-independent WCE, T_w is the mean temperature of water bodies in the study area and T_m is the mean temperature of the whole study area.

Agriculture activities changed the land use/cover patterns, and then had a significant impact on regional mean temperature and UHI. With the impact of human activities, the season-independent and human-dependent urban heat island (RUHI) effect is calculated by Eq. (13). RUHI is influenced by human activities, but not seasonal effect.

$$RUHI = (T_{bu} - T_m) / T_m \tag{13}$$

where RUHI is season-independent and human-dependent urban heat island and T_m is the mean temperature of the entire study area, including the temperature of water bodies.

3.3. Correlation analysis method

Regression analysis methods, such as linear, polynomial, power, and exponential are used for discovering relationships between WCE parameters and landscape scale characteristics of water bodies. The optimal relationship model is determined by the comparison of correlation coefficients (R^2) from each fitting results. The effectiveness of the optimal regression model depends on sample sizes. The effective samples (N) of the Poyang Lake and Dongting Lake regions are 31 and 21, respectively. Based on these sample sizes, the correlations are considered to be significant when correlation coefficients (R^2) are larger than 0.129 (i.e., $R^2 > 4/N$, $N = 31$, $P = 0.05$) and 0.1905 (i.e., $R^2 > 4/N$, $N = 21$, $P = 0.05$) for the Poyang Lake and Dongting Lake regions, respectively [46].

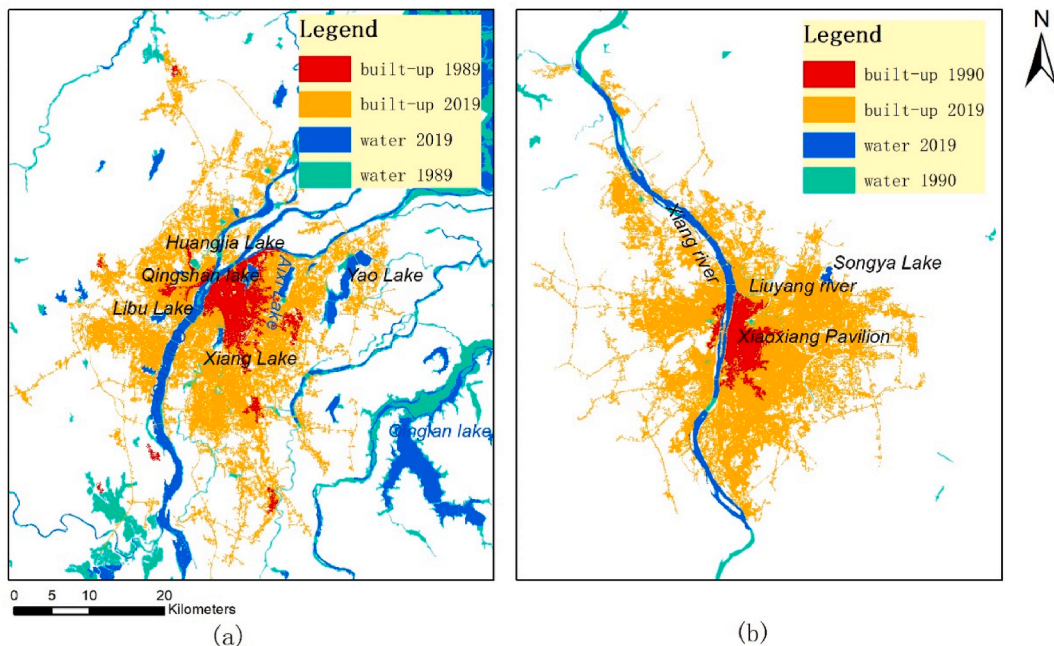


Fig. 6. Spatio-temporal distribution maps of built-up areas and infill water bodies from 1989 to 2019 in: (a) Nanchang; (b) Changsha. NOTE: “water 1989” and “water 1990” refer to the water areas in 1989 and 1990 larger than that in 2019, respectively.

4. Results

4.1. Relationships between urban inside water bodies and their cooling effect

4.1.1. Spatio-temporal distribution of urban inside water bodies

Urban inside water bodies increased with urban sprawl from 1989 to 2019. Fig. 6 shows the spatiotemporal variation of built-up areas and urban inside water bodies from 1989 to 2019. The water bodies are relatively evenly distributed across the urban area of Nanchang (Fig. 6(a)). Nanchang had three main urban inside water bodies in 1989, including, Qingshan Lake, part of Xiang Lake and the Gan River. An increasing amount of water bodies later became surrounded by built-up areas as urban expansion progressed (Table 4). Kongmu, Libu, Huangjia, Aixi, and part of Yao lakes had changed into urban inside water bodies in Nanchang by the end of 2019. The Liuyang River and Songya Lake became urban inside water bodies in Changsha by 2019 (Fig. 6(b)). The urban inside water bodies area increased 34.96 km² and 43.96 km² for Nanchang and Changsha, respectively (Table 4). The increased water bodies mainly is along Xiang river at Changsha. However, the increased of urban inside water bodies distribute throughout the urban area evenly at Nanchang (Fig. 6(a) and (b)).

Areas of specific water bodies decreased with urban sprawl from 1989 to 2019. Some branches of specific lakes (water 1989 in Fig. 6(a)) were converted from water to land (including built-up areas) during the period of 1989–2019, such as Xiang, Aixi and Yao lakes. The area variations of outside discrete water bodies are caused by different seasons of image acquisition time (Table 1), such as Qinglan Lake (Fig. 6(a)). Smaller area changes of water bodies occurred due to urban expansion of Changsha from 1990 to 2019 (0.51 km²), except for along the Xiang River (Fig. 6(b) and Table 4).

The average water depth of urban inside lakes is 3.65 m and 2.18 m in Nanchang and Changsha, respectively. While the mean water depth of Gan River and Xiang River is 4.85 m and 6.91 m, respectively.

4.1.2. Relationship between AR_{wb} and RTD_{bw}

There is no obvious change trend of AR_{wb} in Nanchang since 1989. However, the AR_{wb} of Changsha is decreasing since 1990 (Fig. 7). RTD_{bw} is significant correlated with AR_{wb} for Nanchang and Changsha (Fig. 8). Negative linear relationship is observed between RTD_{bw} and AR_{wb} in Nanchang, whose correlation coefficients (R²) is equal to 0.2594. The value of RTD_{bw} is increasing with the decrease of AR_{wb} in Nanchang except for some days, which is cloudy (May 13th, 2001) or sudden changes in daily temperature (e. g., Jan. 11th, 2009 and Mar 5th, 2005). Two clusters are appeared in Changsha except for cloudy days (Jun. 23rd, 2005 and Apr. 20th, 2005). There is significant negative correlation between RTD_{bw} and AR_{wb}, when AR_{wb} is larger than 0.135 in Changsha (before 2001). However positive linear correlations between RTD_{bw} and AR_{wb} is observed in Changsha, when AR_{wb} is less than 0.135 (after 2001) (Fig. 8).

4.2. Correlations between outside discrete water bodies and their cooling effect

The relationships between outside discrete water bodies and three WCE parameters are explored in this section. Both the acreage and DWAI of outside discrete water bodies (D_σ) are used to describe the landscape scale characteristics of outside discrete water bodies. The acreage of outside discrete water bodies is significant negative correlated with RTD_{bw}, when RTD_{bw} is less than 0.4 in Poyang Lake region. However, there is little correlations between acreage and the other WCE parameters both in Poyang Lake and Dongting Lake regions (Fig. 9).

Different relationships are observed between D_σ and three WCE parameters. There is a significant negative linear relationship between D_σ and RTD_{bw} both in the Poyang Lake and Dongting Lake regions (Fig. 10(b)). However, D_σ is not significant correlated with RUHI and TD_{bw} in both the Poyang Lake and Dongting Lake regions (Fig. 10 (a) & (c)). The RTD_{bw} decreases with the increasing of D_σ both in Poyang and Dongting lake regions. Two clusters are appeared according to flood (June to September) and dry (October to December) seasons in Dongting lake regions (Fig. 10 (b)). The acreage of outside discrete water bodies shows large negative and positive anomaly on June 23rd, 2005 and March 1st, 2016, respectively (Fig. 11). Therefore, the data on June 23rd, 2005 and March 1st, 2016 are combined with clusters of dry and flood seasons, respectively. The regression line between D_σ and TD_{bw} at flood season is approximately parallel with that at dry season. However, the intercept of regression line at flood season is larger than that at dry season (Fig. 10(b)).

4.3. Relationship between large water bodies and WCE

A quadratic polynomial relationship is observed between the acreage of the large water bodies and TD_{bw}, the same as seen between

Table 4
Acreage of urban infill water bodies in Nanchang and Changsha (km²).

Nanchang	Changsha			1990	2019	Total area	Xiang river	Except Xiang
	Toal area	Gan river	Except Gan					
1989	30.176	15.06	15.116			14.688	12.775	1.913
2019	65.14	28.215	36.925			58.65	56.227	2.423

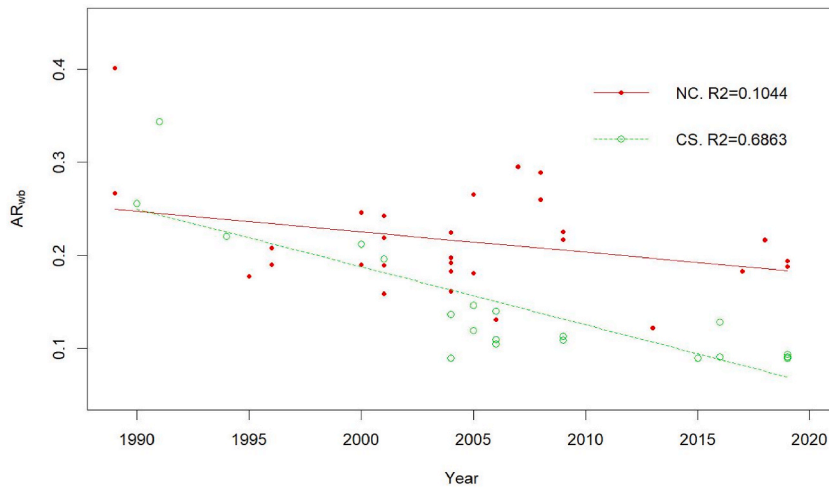


Fig. 7. Time series changes of AR_{wb} for Nanchang (NC) and Changsha (CS).

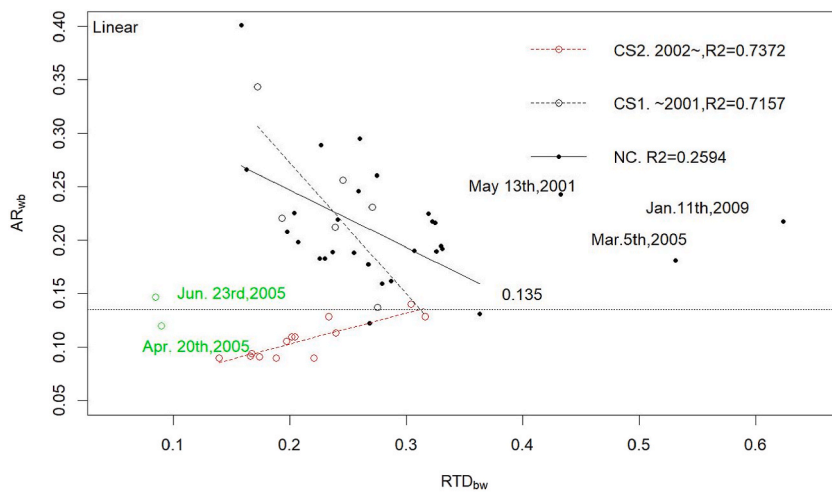


Fig. 8. Relationships between RTD_{bw} and AR_{wb} for Nanchang (NC) and Changsha (CS).

the acreage of large water bodies and RUHI (Fig. 12(a) and (c)). There is no significant correlation between the acreage of large water bodies and RTD_{bw} (Fig. 12(b) and Table 5). The lake acreage is significantly correlated with TD_{bw} for both Poyang Lake and Dongting Lake regions ($P < 0.01$). The correlation coefficients (R^2) between lake acreage and TD_{bw} are equal to 0.282 ($P < 0.01$) and 0.4088 ($P < 0.01$) for Poyang Lake and Dongting Lake regions, respectively (Fig. 12(a) and Table 5). Meanwhile, there are also significant correlations between lake acreage and RUHI for Poyang Lake and Dongting Lake ($P < 0.001$) (Fig. 12(c) and Table 5). The R^2 values between lake acreage and RUHI are equal to 0.4496 ($n = 31, P < 0.001$) and 0.6188 ($n = 21, P < 0.001$) (Fig. 12(c) for Poyang Lake and Dongting Lake regions, respectively). The DWAI of large water bodies (G_{σ}) is significant quadratic correlated with TD_{bw} and RUHI but not RTD_{bw} for Poyang Lake and Dongting Lake regions, respectively (Fig. 13(a), (b) and (c)). Their correlation coefficients are approximately equal to those between lake acreage and TD_{bw} (Figs. 12(a) and 13(a)) and between lake acreage and RUHI ($P < 0.001$) (Figs. 12(c) and 13(c)).

5. Discussion

5.1. The climate adaptive characteristics of urban inside water bodies

The spatial patterns of urban inside water bodies have a more significant effect on RTD_{bw} than their size in the study areas. Some literatures reported that the cooling effect of water bodies was influenced by their sizes [26,28]. The acreage of urban inside water bodies increases both in Nanchang and Changsha (Table 4). However, the relationship between AR_{wb} and RTD_{bw} in Nanchang is different from that in Changsha (Section 4.1.2). This difference is due to their difference in spatial patterns of urban inside water

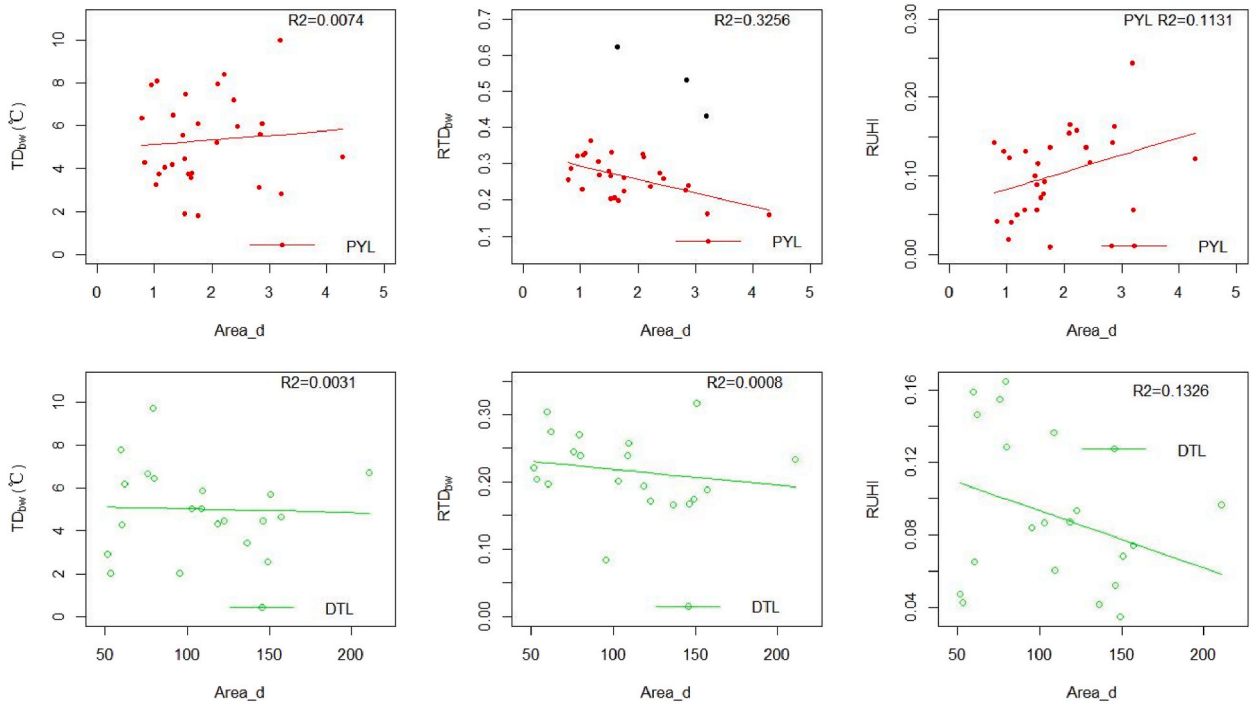


Fig. 9. Relationships between acreage of outside discrete water bodies (*Area_d*) and UHI in Poyang Lake (PYL) and Dongting Lake (DTL) regions.

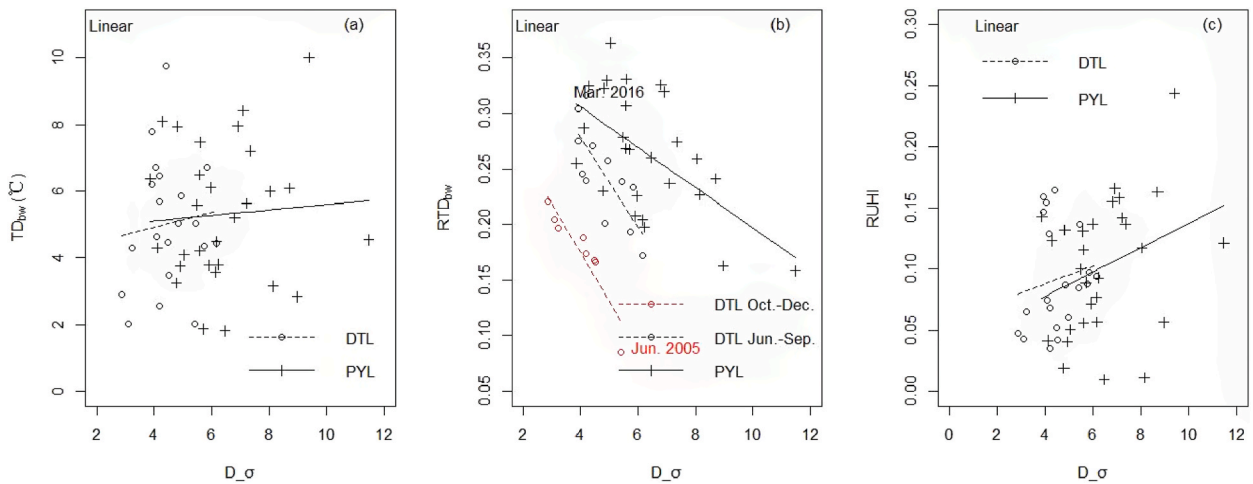


Fig. 10. Relationships between DWAI of outside discrete water bodies (D_σ) and UHI in Poyang Lake (PYL) and Dongting Lake (DTL) regions: (a) D_σ and TD_{bw} ; (b) D_σ and RTD_{bw} ; (c) D_σ and $RUHI$.

bodies, which has a significant impact on UHI [16,25]. The Changsha before 2001 and Nanchang since 1989 were characterized by “waterfront city surrounded by rivers and lakes” (Figs. 6(a) and Fig. 14(a)), which decline WCE of urban inside water bodies. Therefore, the relationship between RTD_{bw} and AR_{wb} in Changsha before 2001 is same to that in Nanchang since 1989. However, the relationship between RTD_{bw} and AR_{wb} in Changsha before 2001 is different from that since 2001 (Figs. 8 and 14(b)).

The different relationship for the two clusters in Changsha (Fig. 8) is influenced by the landscape patterns of urban water bodies. The urban sprawl of Changsha had been changed the landscape patterns of urban water bodies, especially since 2003. The PARA of urban inside water bodies increases with the increasing of AR_{wb} in Changsha since 2001, when AR_{wb} is less than 0.2302 (Fig. 15(a) and (b)). However, the PARA of urban inside water bodies decreases with the increasing of AR_{wb} in Changsha before 2001, when AR_{wb} is larger than 0.2302 (Fig. 15(b)). It is known that AR_{wb} of Changsha had been decreased since 1990 (Fig. 7). It is obvious that the landscape patterns of urban inside water bodies have more significant effect on RTD_{bw} than their size in the study areas, which is seldom discussed in the former studies [29]. PARA of urban inside water bodies is positively correlated with their WCE. The urban

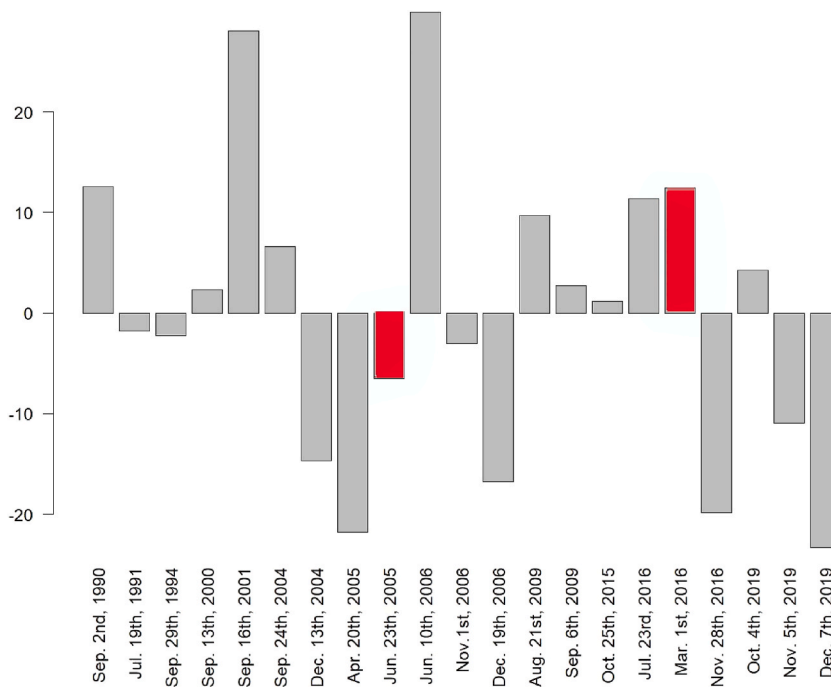


Fig. 11. Area Anomaly of outside discrete water bodies from 1990 to 2019.

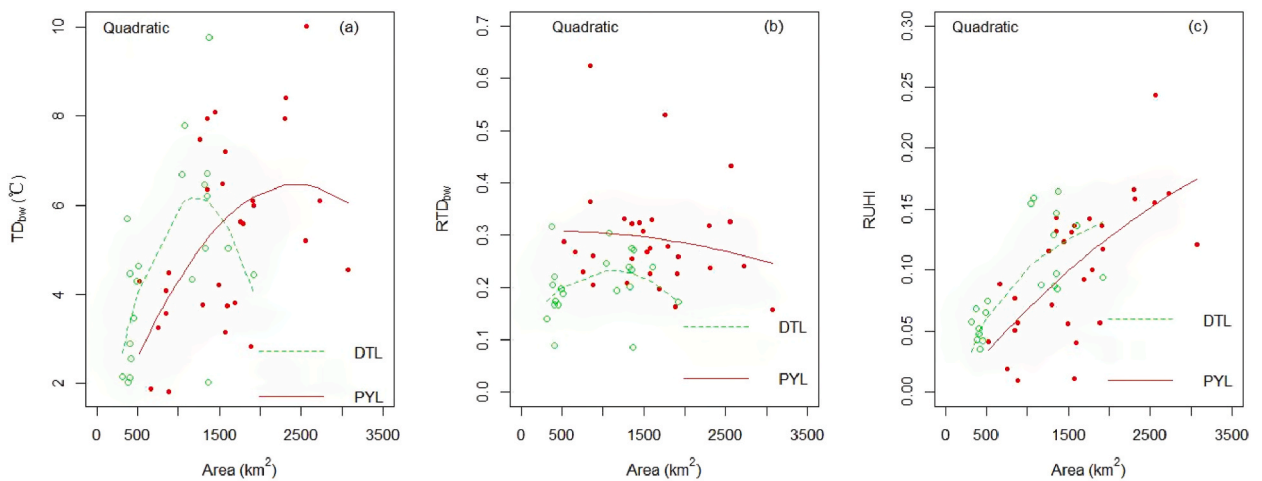


Fig. 12. Relationships between large lake acreage and the urban heat island effect: (a) Area and TD_{bw} ; (b) Area and RTD_{bw} ; (c) Area and RUHI.

inside water bodies with long shape should be increased in the planning of urban blue spaces. The cooling effect of flowing river water bodies is higher than that of static lake water bodies, which might be caused by their difference in water depth. The average water depth of flowing river is deeper than that of static lake (Section 4.1.1). The orientation of Xiang River might enhance its cooling effect because of its prevail wind direction in Dongting Lake regions [39].

5.2. The climate adaptive characteristics of urban outside discrete water bodies

The acreage of outside discrete water bodies have little influence on WCE parameters, other than on RTD_{bw} in Poyang lake region (Fig. 9). The WCE decreased with the increasing of their distance from built-up areas [13,30]. Actually, significant negative linear relationships have been found between D_{σ} and RTD_{bw} both in Poyang and Dongting lake regions (Fig. 10(b)). In other words, outside discrete water bodies have significant influence on RTD_{bw} (Fig. 10(b)), but not on TD_{bw} (Fig. 10(a)) and RUHI (Fig. 10(c)). However, it is related with season and size of water bodies. The seasonal WCE have been found at coastal cities [33], the same to Dongting Lake region. The WCE varies with their D_{σ} within a season rather than acreage (Fig. 10(b)). RTD_{bw} is significant negative linear correlated

Table 5
Appendix table for regression equations.

Variables	Study area	Equation	R ²	R-Figures
Year and AR _{wb}	NC	$y = -0.0022x + 4.5864$	0.1044	
RTD _{bw} and AR _{wb}	CS	$y = -0.0062x + 12.614$	0.6863	Fig. 7
	NC	$y = -0.5357x + 0.354$	0.2594	Fig. 8
	CS	$y = -1.2275x + 0.5179$	0.7157	
D _σ and TD _{bw}	CS	$y = 0.2876x + 0.0453$	0.7372	
	PYL	$y = 0.0823x + 4.7785$	0.0047	Fig. 10(a)
	DTL	$y = 0.4893x + 2.5564$	0.0439	
D _σ and RTD _{bw}	PYL	$y = -0.0181x + 0.3782$	0.3323	Fig. 10(b)
	DTL	$y = -0.0403x + 0.4393$	0.5801	
	DTL	$y = -0.045x + 0.3523$	0.8286	Fig. 10(c)
D _σ and RUHI	PYL	$y = 0.0099x + 0.0378$	0.0985	
	DTL	$y = 0.0041x + 0.0735$	0.078	
	PYL	$y = -1E-6x^2 + 0.005x + 0.3207$	0.282	Fig. 12 (a)
Area and TD _{bw}	DTL	$y = -4E-06x^2 + 0.0103x - 0.0982$	0.4088	
	PYL	$y = 0.3172e^{-8E-05x}$	0.0318	Fig. 12(b)
	DTL	$y = -9E-08x^2 + 0.0002x + 0.1206$	0.1271	
Area and RTD _{bw}	PYL	$y = -7E-09x^2 + 8E-05x - 0.0062$	0.4496	Fig. 12(c)
	DTL	$y = -9E-08x^2 + 0.0002x - 0.0397$	0.6188	
	PYL	$y = -0.0036x^2 + 0.2971x + 0.4008$	0.2746	Fig. 13(a)
Area and RUHI	DTL	$y = -0.0443x^2 + 1.051x - 0.0531$	0.4185	Fig. 13(a)
	PYL	$y = 0.3178e^{-0.005x}$	0.0337	Fig. 13(b)
	DTL	$y = -0.001x^2 + 0.0214x + 0.1176$	0.1435	
G _σ and TD _{bw}	PYL	$y = 3E-05x^2 + 0.051x - 0.0082$	0.4494	Fig. 13(c)
	DTL	$y = -0.0009x^2 + 0.0243x - 0.0354$	0.6147	
	PYL	$y = -10.627x^2 + 5.9675x + 0.0086$	0.385	Fig. 15(a)
AR _{wb} and PARA	NC	$y = -18.742x^2 + 8.6305x - 0.1621$	0.4804	Fig. 15(b)
	CS			

Note: PYL refers Poyang lake regions and DTL is Dongting lake regions; R² is the correlation coefficients; R-Figures is the related figures; D_σ is the distance-weighted area index of outside discrete water bodies; G_σ the distance-weighted area index of large water bodies.

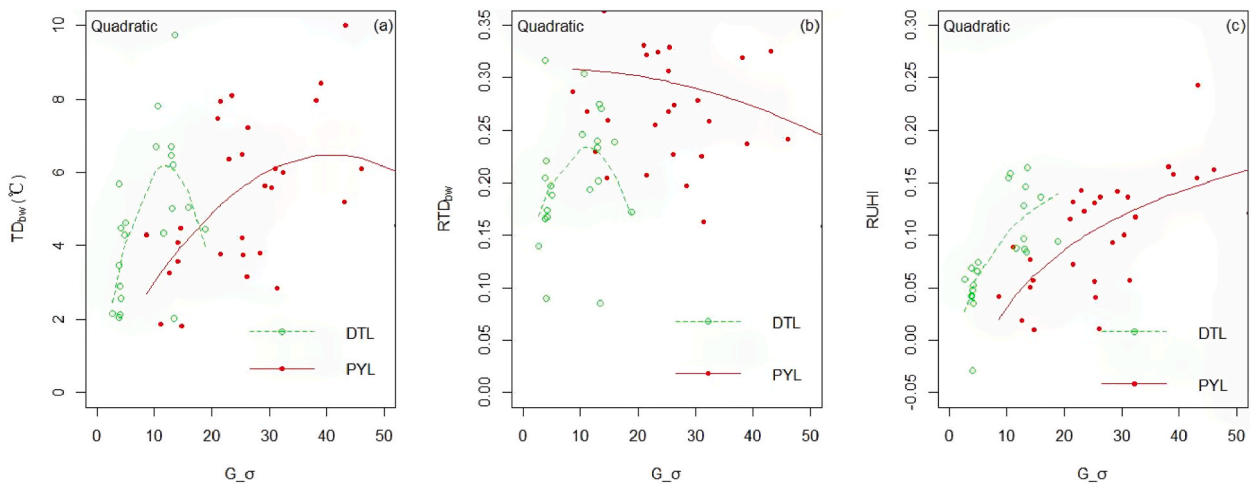


Fig. 13. Relationship between DWAI of large water bodies (G_{σ}) and UHI: (a) G_{σ} and TD_{bw} ; (b) G_{σ} and RTD_{bw} ; (c) G_{σ} and $RUHI$.

with D_{σ} both at flood and dry seasons. The value of RTD_{bw} at flood season is larger than that at dry season, when D_{σ} is a certain value. This inter-seasonal difference of RTD_{bw} is caused by seasonal water levels. The cooling effect of outside discrete water bodies is influenced by their distance from built-up area and water volume. However, it is opposite with the former studies, which found negative relationship between water bodies' distance from built-up area and WCE [29]. In this work, positive relationship is found between their distance from built-up area and WCE. The closer the distance from built-up area, the smaller the WCE, which might be caused by human activities. The larger the water volume, the larger the WCE. In other word, the deep-water landscape should be increased to enhance the cooling effect of blue spaces outside the cities.

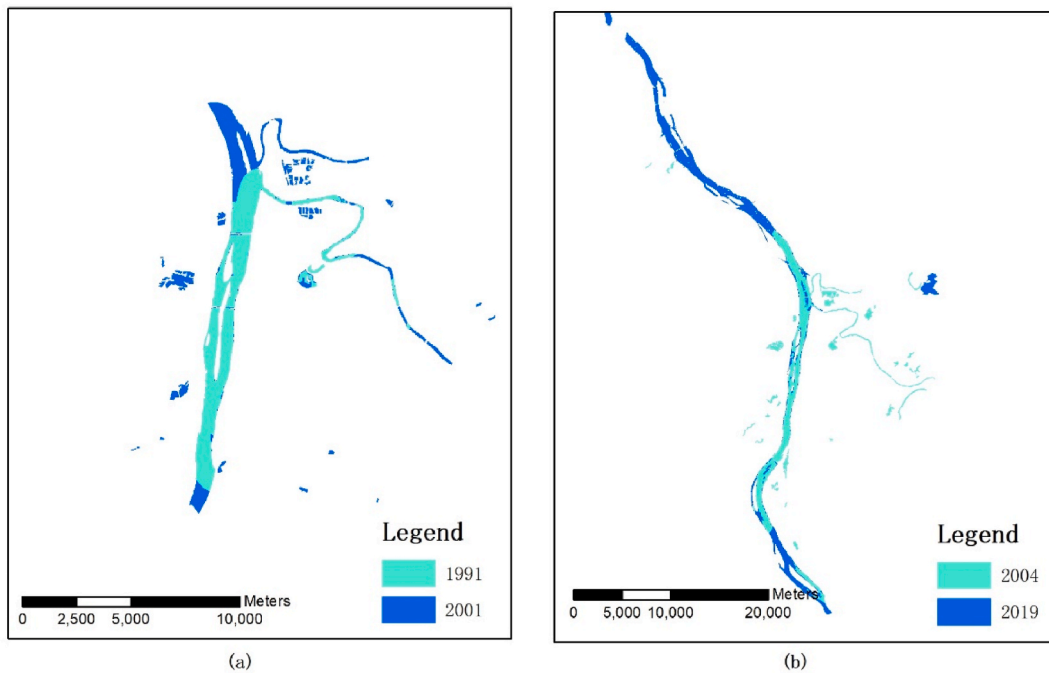


Fig. 14. Sprawl of urban inside water bodies in Changsha: (a) before 2001; (b) since 2001.

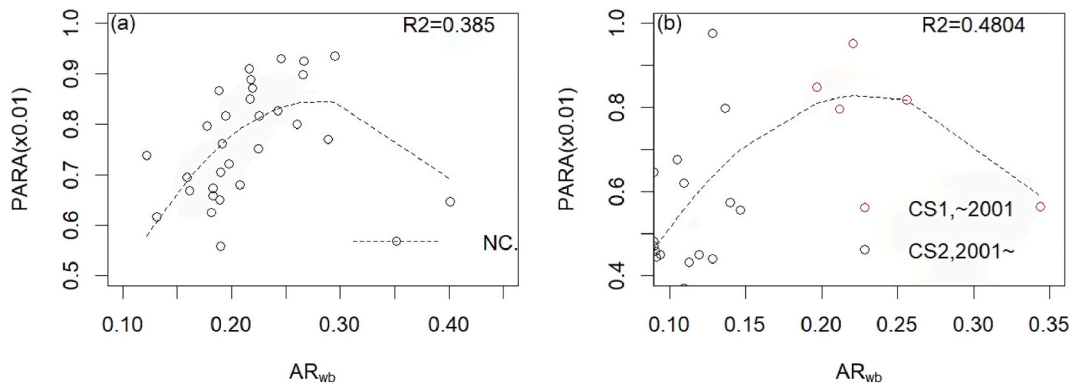


Fig. 15. Relationships between AR_{wb} and Perimeter-to-area ratio (PARA) for Nanchang (NC) and Changsha (CS).

5.3. The climate adaptive characteristics of large water bodies

Human activities and climate conditions have significant influence on WCE both in Poyang Lake and Dongting Lake regions. The spatial patterns and acreage of large water bodies have a more significant influence on TD_{bw} than that on RTD_{bw} , which indicate changing climate condition enhance the cooling effect of large water bodies on UHI. The correlation coefficient between large water bodies and RUHI is larger than that between large water bodies and TD_{bw} , which indicate human activities have a more significant influence than the changing climate condition on WCE. Reference [18] found that water bodies would enhance the cooling effect of trees. Oppositely, green spaces would enhance WCE. The agricultural activities, as the main human activities in the study area, change the agricultural green spaces, and then enhance WCE.

The impact on WCE has little difference between G_{σ} and acreage of large water bodies. This little difference might be caused by the little distance changes from large water bodies to urban centers for the last three decades.

A negative logarithmic relationship had been published between urban water body size and mean land surface temperature [27]. The quadratic polynomial relationships exhibit between WCE and outside large water bodies (Fig. 12 (a)). TD_{bw} reach the maximum value, when the acreage of Poyang and Dongting Lake is equal to 2500 and 1287.5 square kilometers, respectively (Fig. 12(a) and Table 5). Meanwhile, RUHI reach the top value, when the acreage of Poyang and Dongting Lake is approximately equal to 5714 and 1111 square kilometers, respectively (Fig. 12(c) and Table 5). It is recorded that the maximum acreage of Poyang lake is 4206 km².

Generally, RUHI is significant positive correlated with the acreage of Poyang Lake. The ideal acreage is larger than 2500 km² for climate adaption of Poyang Lake. And the ideal acreage of east and south Dongting Lake is 1111–1287.5 km² for climate adaption.

6. Conclusions

Multi-temporal Landsat TM/OLI/TIRS images are used to explore the climate adaptive characteristics of water bodies based on their cooling effect in the Poyang Lake and Dongting Lake regions. It is found that the climate adaptive characteristics of urban inside water bodies are shape, depth, orientation and fluidity of water bodies. The urban inside water bodies with long shape, located upwind should be increased to enhance their cooling effect. Simultaneously, the cooling effect of flowing water bodies is higher than that of static water bodies inside cities. For urban outside discrete water bodies in our study areas, their distance from built-up areas and water depth are advised to increase for regional climate adaption. The climate adaption of the study areas is enhanced, when the acreage of Poyang Lake and Dongting Lake is limited in an ideal threshold (Section 5.1).

This study focused on the influence of water bodies on regional climate adaption, but not on cooling of UHI. Therefore, some conclusions in this work seem opposite with previous studies. For example, the outside discrete water bodies near built-up areas have smaller cooling effect than that far from built-up areas, which seems opposite with previous studies [13]. Actually, they are consistent with each other. It should be noted that the climate adaptive characteristics of water bodies are influenced by human activities and climate conditions, especially for large water bodies far from built-up areas.

The satellite transit time in our study domain is ~9:45AM for Landsat TM/OLI. It is known that the ecological effect of water bodies varies with the time of day. In future work, daily time series data would be employed to better understand the climate adaptive characteristics of water bodies.

Author contribution statement

Zhigang Deng: Performed the experiments; Analyzed and interpreted the data; Wrote the paper.

Hongmei Zhao: Conceived and designed the experiments; Analyzed and interpreted the data.

Lin Li, Guihua Liu, Hui Lin: Contributed reagents, materials, analysis tools or data.

Adam Thomas DEVLIN: Contributed reagents, materials, analysis tools or data; Wrote the paper.

Funding

This work was supported by the Natural Science Foundation of China (42161062, 41461079) and the Opening Fund of Key Laboratory of Poyang Lake Wetland and Watershed Research (Jiangxi Normal University), Ministry of Education (No. PK2020001).

Data availability statement

Data associated with this study has been deposited at The Landsat TM/OLI/TIRS data that support the findings of this study are openly available in Google Earth Engine and <http://www.gscloud.cn>. The classification and statistical data, including radiance temperature and water areas, are available from the corresponding author.

Declaration of competing interest

The authors declare that they have no known competing financial interests or personal relationships that could have appeared to influence the work reported in this paper.

References

- [1] C.P. Lo, D.A. Quattrochi, J.C. Luvall, Application of high-resolution thermal infrared remote sensing and GIS to assess the urban heat island effect, *Int. J. Rem. Sens.* 18 (2) (1997) 287–304, <https://doi.org/10.1080/014311697219079>.
- [2] P. Singh, N. Kikon, P. Verma, Impact of land use change and urbanization on urban heat island in Lucknow city, Central India. A remote sensing based estimate, *Sustain. Cities Soc.* 32 (2017) 100–114, <https://doi.org/10.1016/j.scs.2017.02.018>.
- [3] A.N. Moyer, T.W. Hawkins, River effects on the heat island of a small urban area, *Urban Clim.* 21 (2017) 262–277, <https://doi.org/10.1016/j.uclim.2017.07.004>.
- [4] F.W. Leal, I.L. Echevarria, A. Neht, et al., Coping with the impacts of urban heat islands. A literature based study on understanding urban heat vulnerability and the need for resilience in cities in a global climate change context, *J. Clean. Prod.* 171 (2018) 1140–1149, <https://doi.org/10.1016/j.jclepro.2017.10.086>.
- [5] X. Sun, X. Tan, K. Chen, et al., Quantifying landscape-metrics impacts on urban green-spaces and water-bodies cooling effect: the study of Nanjing, China, *Urban For. Urban Gree.* 55 (2020), 126838, <https://doi.org/10.1016/j.ufug.2020.126838>.
- [6] Y. Lin, Z. Wang, C.Y. Jim, et al., Water as an urban heat sink: blue infrastructure alleviates urban heat island effect in mega-city agglomeration, *J. Clean. Prod.* 262 (2020), 121411, <https://doi.org/10.1016/j.jclepro.2020.121411>.
- [7] S. Völker, T. Kistemann, The impact of blue space on human health and well-being—Salutogenetic health effects of inland surface waters: a review, *Int. J. Hyg. Environ. Health* 214 (6) (2011) 449–460, <https://doi.org/10.1016/j.ijheh.2011.05.001>.
- [8] S. Völker, J. Matros, T. Claßen, Determining urban open spaces for health-related appropriations: a qualitative analysis on the significance of blue space, *Environ. Earth Sci.* 75 (13) (2016) 1–18, <https://doi.org/10.1007/s12665-016-5839-3>.
- [9] J.K. Garrett, M.P. White, J. Huang, et al., Urban blue space and health and wellbeing in Hong Kong: results from a survey of older adults, *Health Place* 55 (2019) 100–110, <https://doi.org/10.1016/j.healthplace.2018.11.003>.

- [10] Y. Chen, Y. Yuan, The neighborhood effect of exposure to blue space on elderly individuals' mental health: a case study in Guangzhou, China, *Health Place* 63 (2020), 102348, <https://doi.org/10.1016/j.healthplace.2020.102348>.
- [11] R. Costanza, R. S. Groot, S. Farber, Paruelo, et al., The value of the world's ecosystem services and natural capital, *Nature* 387 (1997) 253–260, [https://doi.org/10.1016/S0921-8009\(98\)00020-2](https://doi.org/10.1016/S0921-8009(98)00020-2).
- [12] C. Wang, W. Zhu, Analysis of the impact of urban wetland on urban temperature based on remote sensing technology, *Procedia Environ. Sci.* 10 (2011) 1546–1552, <https://doi.org/10.1016/j.proenv.2011.09.246>.
- [13] Z. Cai, G. Han, M. Chen, Do water bodies play an important role in the relationship between urban form and land surface temperature? *Sustain. Cities Soc.* 39 (2018) 487–498, <https://doi.org/10.1016/j.scs.2018.02.033>.
- [14] N. Gupta, A. Mathew, S. Khandelwal, Analysis of cooling effect of water bodies on land surface temperature in nearby region: a case study of Ahmedabad and Chandigarh cities in India, Egypt, *J. Remote Sens.* 22 (1) (2019) 81–93, <https://doi.org/10.1016/j.ejrs.2018.03.007>.
- [15] D. Zhu, X. Zhou, W. Cheng, Water effects on urban heat islands in summer using WRF-UCM with gridded urban canopy parameters-A case study of Wuhan, *Build. Environ.* 225 (2022), 09528, <https://doi.org/10.1016/j.buildenv.2022.109528>.
- [16] R. Sun, A. Chen, L. Chen, Y. Lü, Cooling effects of wetlands in an urban region: the case of Beijing, *Ecol. Indic.* 20 (2012) 57–64, <https://doi.org/10.1016/j.ecolind.2012.02.006>.
- [17] X. Xue, T. He, L. Xu, et al., Quantifying the spatial pattern of urban heat islands and the associated cooling effect of blue-green landscapes using multisource remote sensing data, *Sci. Total Environ.* 843 (2022), 156829, <https://doi.org/10.1016/j.scitotenv.2022.156829>.
- [18] D. Shi, J. Song, J. Huang, et al., Synergistic cooling effects (SCEs) of urban green-blue spaces on local thermal environment: a case study in Chongqing, China, *Sustain. Cities Soc.* 55 (2020), 102065, <https://doi.org/10.1016/j.scs.2020.102065>.
- [19] J. Peng, Y. Dan, R. Qiao, et al., How to quantify the cooling effect of urban parks? Linking maximum and accumulation perspectives, *Remote Sens. Environ.* 252 (2021), 112135, <https://doi.org/10.1016/j.rse.2020.112135>.
- [20] A.M. Couttset, N.J. Tapper, J. Beringer, et al., Watering our cities: the capacity for water sensitive urban design to support urban cooling and improve human thermal comfort in the Australian context, *Prog. Phys. Geogr.* 37 (2013) 2–28, <https://doi.org/10.1177/0309133312461032>.
- [21] G.J. Steeneveld, S. Koopmans, B.G. Heusinkveld, et al., Refreshing the role of open water surfaces on mitigating the maximum urban heat island effect, *Lands. Urban Plann.* 121 (2014) 92–96, <https://doi.org/10.1016/j.landurbplan.2013.09.001>.
- [22] Z. Wu, Y. Zhang, Water bodies' cooling effects on urban land daytime surface temperature: ecosystem service reducing heat island effect, *Sustainability* 11 (3) (2019) 787, <https://doi.org/10.3390/su11030787>.
- [23] D. Nutsford, A.L. Pearson, S. Kingham, et al., Residential exposure to visible blue space (but not green space) associated with lower psychological distress in a capital city, *Health Place* 39 (2016) 70–78, <https://doi.org/10.1016/j.healthplace.2016.03.002>.
- [24] X. Tan, X. Sun, C. Huang, et al., Comparison of cooling effect between green space and water body, *Sustain. Cities Soc.* 67 (2021), 102711, <https://doi.org/10.1016/j.scs.2021.102711>.
- [25] J. Li, C. Song, L. Cao, Impact of landscape structure on surface urban heat islands: a case study of Shanghai, China, *Remote Sens. Environ.* 115 (2011) 3249–3263, <https://doi.org/10.1016/j.rse.2011.07.008>.
- [26] S.V. Smith, W.H. Renwick, J.D. Bartley, et al., Distribution and significance of small, artificial water bodies across the United States landscape, *Sci. Total Environ.* 299 (1–3) (2002) 21–36, [https://doi.org/10.1016/S0048-9697\(02\)00222-X](https://doi.org/10.1016/S0048-9697(02)00222-X).
- [27] C. Wu, J. Li, C. Wang, et al., Understanding the relationship between urban blue infrastructure and land surface temperature, *Sci. Total Environ.* 694 (2019), 133742, <https://doi.org/10.1016/j.scitotenv.2019.133742>.
- [28] J. Peng, Q. Liu, Z. Xu, et al., How to effectively mitigate urban heat island effect? A perspective of waterbody patch size threshold, *Lands. Urban Plann.* 202 (2020), 103873, <https://doi.org/10.1016/j.landurbplan.2020.103873>.
- [29] R. Sun, L. Chen, How can urban water bodies be designed for climate adaptation, *Lands. Urban Plann.* 105 (1–2) (2012) 27–33, <https://doi.org/10.1016/j.landurbplan.2011.11.018>.
- [30] S. Cheval, A.M. Popa, I. Sandric, et al., Exploratory analysis of cooling effect of urban lakes on land surface temperature in Bucharest (Romania) using Landsat imagery, *Urban Clim.* 34 (2020), 100696, <https://doi.org/10.1016/j.uclim.2020.100696>.
- [31] Y. Cui, L. Hu, Z. Wang, et al., Urban nocturnal cooling mediated by bluespace, *Theor. Appl. Climatol.* 146 (2021) 277–292, <https://doi.org/10.1007/s00704-021-03727-5>.
- [32] J. Wu, C. Li, X. Zhang, et al., Seasonal variations and main influencing factors of the water cooling islands effect in Shenzhen, *Ecol. Indic.* 117 (2020), 106699, <https://doi.org/10.1016/j.ecolind.2020.106699>.
- [33] J. Suomi, J. Kayhko, The impact of environmental factors on urban temperature variability in the coastal city of Turku, SW Finland, *Int. J. Climatol.* 32 (2012) 451–463, <https://doi.org/10.1002/joc.2277>.
- [34] G. Manteghi, H. Limit, D. Remaz, Water bodies an urban microclimate: a review, *Mod. Appl. Sci.* 9 (6) (2015) 1, <https://doi.org/10.5539/mas.v9n6p1>.
- [35] N.I. Syaffii, M. Ichinose, N.H. Wong, et al., Experimental study on the influence of urban water body on thermal environment at outdoor scale model, vol. 169, in: *Fourth International Conference on Countermeasures to Urban Heat Island*, *Procedia Engineering*, 2016, pp. 191–198, <https://doi.org/10.1016/j.proeng.2016.10.023>.
- [36] P. Ampatzidis, T. Kershaw, A review of the impact of blue space on the urban microclimate, *Sci. Total Environ.* 730 (2020), 139068, <https://doi.org/10.1016/j.scitotenv.2020.139068>.
- [37] C. Jacobs, L. Klok, M. Bruse, et al., Are urban water bodies really cooling? *Urban Clim.* 32 (2020), 100607, <https://doi.org/10.1016/j.uclim.2020.100607>.
- [38] K. Yu, Y. Chen, L. Liang, et al., Quantitative analysis of the interannual variation in the seasonal water cooling island (WCI) effect for urban areas, *Sci. Total Environ.* 727 (2020), 138750, <https://doi.org/10.1016/j.scitotenv.2020.138750>.
- [39] E.D. Giuseppe, G. Ulpiani, C. Cancellieri, et al., Numerical modelling and experimental validation of the microclimatic impacts of water mist cooling in urban areas, *Energy Build.* 231 (2021), 110638, <https://doi.org/10.1016/j.enbuild.2020.110638>.
- [40] X. Chen, H. Zhao, P. Li, et al., Remote sensing image-based analysis on the relationship between urban heat island and land use/cover change, *Remote Sens. Environ.* 104 (2) (2006) 133–146, <https://doi.org/10.1016/j.rse.2005.11.016>.
- [41] Q. Huang, J. Huang, X. Yang, et al., Quantifying the seasonal contribution of coupling urban land use types on Urban Heat Island using Land Contribution Index: a case study in Wuhan, China, *Sustain. Cities Soc.* 44 (2019) 666–675, <https://doi.org/10.1016/j.scs.2018.10.016>.
- [42] C.B. Karakuş, The Impact of Land Use/Land Cover (LULC) Changes on land surface temperature in Sivas city center and its surroundings and assessment of urban heat island, *Asia-Pac. J. Atmos. Sci.* 55 (4) (2019) 669–684, <https://doi.org/10.1007/s13143-019-00109-w>.
- [43] Z. Yu, G. Yang, S. Zuo, et al., Critical review on the cooling effect of urban blue-green space: a threshold-size perspective, *Urban For. Urban Gree.* 49 (2020), 126630, <https://doi.org/10.1016/j.ufug.2020.126630>.
- [44] K. McGarigal, B.J. Marks FRAGSTATS, Spatial Pattern Analysis Program for Quantifying Landscape Structure, U.S. Dept. of Agriculture, Forest Service, Pacific Northwest Research Station, 1995.
- [45] S. Jia, D. Xue, C. Li, et al., Study on new method for water area information extraction based on Sentinel-1 data, *Yangtze River* (No.2) (2019) 213–217, <https://doi.org/10.16232/j.cnki.1001-4179.2019.02.038>.
- [46] G.J. Glasser, R.F. Winter, Critical values of the coefficient of rank correlation for testing the hypothesis of independence, *Biometrika* 48 (3/4) (1961) 444–448, <https://doi.org/10.2307/2332767>.